Nuclear Metal Fuel: Characteristics, Design, Manufacturing, Testing, and Operating History

Prepared by the Fast Reactor Working Group

White Paper 18-01

June 2018

INTRODUCTION

This paper is a primer on metal fuel historical use, design, characteristics, physical considerations, testing and operational history, and related analytical tools. This paper was prepared by the Fast Reactor Working Group (FRWG) to inform the Nuclear Regulatory Commission (NRC) staff on the state of the art with respect to metal fuels. As of the submission of this document, the FRWG currently has 7 members who intend to use metal fuels in their designs. This paper has been designed to be technology neutral for any reactor design intending to use metal fuels and as such will help inform the NRC staff in future interactions with any such applicant or pre-applicant. While the NRC has recently developed draft non-light water reactor design criteria, this information can be useful for discussions with pre-applicants regarding principal design criteria, source term, PRA, and a host of other topics, since fuel behavior is at the core of the safety analysis of any design. As such, this paper may support NRC efforts outlined in the NRC Vision and Strategy document.

Table of Contents

BACKGROUND

Some of the first nuclear reactors constructed in the U.S., such as Experimental Breeder Reactor (EBR)-I, EBR-II, and Fermi-1, utilized metal fuel. Metal fuel consists of a heavy metal (typically uranium) that is alloyed with various other metals for irradiation performance purposes. As with oxide fuel, metal fuel is traditionally contained within cladding that provides structural support and acts as a fission product barrier between the fuel and the coolant. The metal fuel is typically bonded to the cladding by liquid sodium to improve heat transfer characteristics. Some important considerations when selecting materials are (1) the ability of the fuel and the cladding to withstand material damage due to the high-energy neutron flux, (2) the ability to survive design basis events without release of any fission products, and (3) the ability of the fuel-cladding combination to minimize both the release of fission products and subsequent consequences during and after a beyond design basis event. Fuel and cladding materials discussed in this paper include: U-Fs[1], binary metal fuels (i.e., U-Zr), ternary fuels (i.e., U-Pu-Zr), stainless steel (SS) 316, HT9, and D9. Although this paper discusses ternary fuel, the focus is on binary fuel because of its recent interest to the advanced nuclear industry.

Benefits of Metal Fuel

Metal fuel offers benefits that make it well suited for fast-spectrum reactor applications. The thermal conductivity of metal fuel is an order of magnitude higher than that of oxide fuel. This reduces peak temperatures and local hot spots. Metal fuel also has a relatively low heat capacity, which limits the stored heat in the fuel, allowing the fuel to be cooled more readily. Thus, even with the lower melting point of metal fuel relative to oxide fuel, the operating margins to fuel failure can be greater, and the fuel exhibits inherent passive safety characteristics [1].

Another key benefit of metal fuel is that it enables a faster spectrum through its higher heavy metal density. The faster spectrum provides many advantages, including the ability to burn actinides and reduce the waste stream, and to breed additional fuel. These superior neutronic characteristics also enable core designs with a small reactivity loss over the operating life, which can be used to extend core life and improve safety margins.

Additionally, metal fuel is cheaply and easily fabricated. Although injection casting has been one of the most widely used fabrication methods, many techniques have been used [2]. The diversity of fabrication methods demonstrates the versatility of metal fuel design, and the relative simplicity of the methods assist in the recycling of metal fuel, because they allow for automated processing in a hot cell facility.

Importantly, the benefits of metal fuel have been demonstrated in operating reactors, in particular during thirty years of metal fuel experience at EBR-II. This demonstration occurred within the context of practical reactor experience, as EBR-II produced 19 MW of electricity at high capacity factors. The culture of continuous improvement at EBR-II also drove substantial development and advancement of metal fuel.

[1] Fissium (Fs) is an equilibrium concentration of fission product elements left by the pyrometallurgical reprocessing cycle designed for EBR-II. It is an alloy with 5% Fs (i.e., 5Fs), containing 2.4 wt% Mo, 1.9 wt% Ru, 0.3 wt% Rh, 0.2 wt% Pd, 0.1 wt% Zr, and 0.1 wt% Nb.

Metal Fuel Design

Metal fuel elements typically consist of metal fuel ingots or slugs[2], cladding, a thermal bond material for the fuel-cladding interface, a gas plenum, and end plugs. Historically, the most common configuration of metal fuel is a cylindrical pin design, illustrated in Figure 1. Nevertheless, the versatility of metal fuel fabrication enables many different designs. Solid metal fuel slugs, either one full-length slug or a stack of segmented pieces, are loaded inside the cladding. The gap between the fuel slugs and the cladding inner diameter allows for fuel swelling during irradiation (see Fission Gas Release and Fuel Swelling for more information), a critical performance characteristic for metal fuel. Sodium is used to fill the gap, providing a thermal bond until the fuel swells into contact with the cladding. Above the sodium fill level is the fission gas plenum, which allows for the collection of fission gas without excess pressure on the cladding. Finally, end plugs are used to seal the element, preventing gas or sodium release.

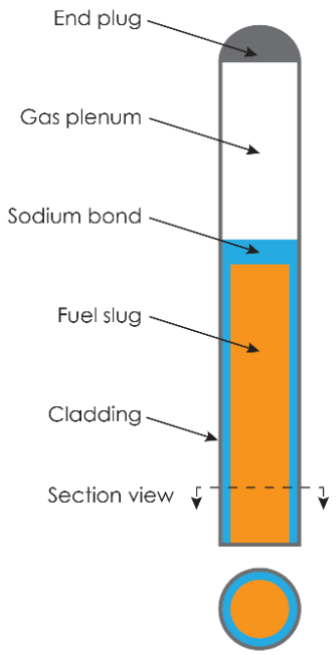

Figure 1. One example of a metal fuel element – cylindrical metal fuel pin.

Two important terms commonly used in metal fuel design are "smear density" and "plenum to fuel volume ratio." The smear density is a unit-less quantity that is the percentage of the theoretical density of the fuel if it were to "smear" radially in the fuel element cross-section. It is also defined as the measure of the cross-sectional area fraction occupied by fuel, or the areal density of the as-fabricated fuel inside the as-fabricated inner-wall surface of the cladding, shown as:

$$Smear\ density = \frac{\rho_{fabricated}}{\rho_{theoretical}} * \frac{A_{fuel}}{A_{element}}$$

Where $\rho_{fabricated}$ is as-fabricated density of the fuel, $\rho_{theoretical}$ is the theoretical density of the fuel, A_{fuel} is the cross-sectional area of the fuel, and $A_{element}$ is the cross-sectional area of the element (taken from the inner wall surface of the cladding). Because the as-fabricated density is typically very

[2] A fuel "slug" is an un-encapsulated, as-fabricated, piece of metal fuel.

close to the theoretical density, it is sometimes omitted in literature. However, it should be included for completeness. It is important for metal fuel designs to have a low enough smear density to properly allow for fuel swelling over the course of fuel life.

The plenum to fuel volume ratio refers to the relative volume of the gas plenum to that of the fuel, calculated as the volume of the plenum region divided by the volume of the fuel region. It is important to size the plenum such that it can accommodate the fission gases released throughout the lifetime of the metal fuel. Therefore, the ratio must be larger for fuel that will reach higher burnups. Alternatively, the cladding wall thickness could be increased to accommodate higher fission gas pressures.

STEADY STATE CONSIDERATIONS

Fission Gas Release and Fuel Swelling

Fuel swelling is a phenomenon driven by the nucleation and growth of fission gas bubbles (mainly xenon and krypton). These fission gasses are virtually insoluble in the fuel matrix, so they are rejected from the matrix and form small bubbles. The accumulation of these gas bubbles causes the fuel to expand due to internal swelling. The morphology of the fission gas bubbles is visible in Figure 2, where dark areas are the fission gas bubbles [3]. In early metal fuel designs swelling was severe enough to fail the cladding, and was the primary factor in limiting fuel lifetime (see Fuel-Cladding Mechanical Interaction for more information). However, later designs solved this problem by reducing the smear density to allow sufficient room for swelling to take place, and eliminated failures due to this phenomenon.

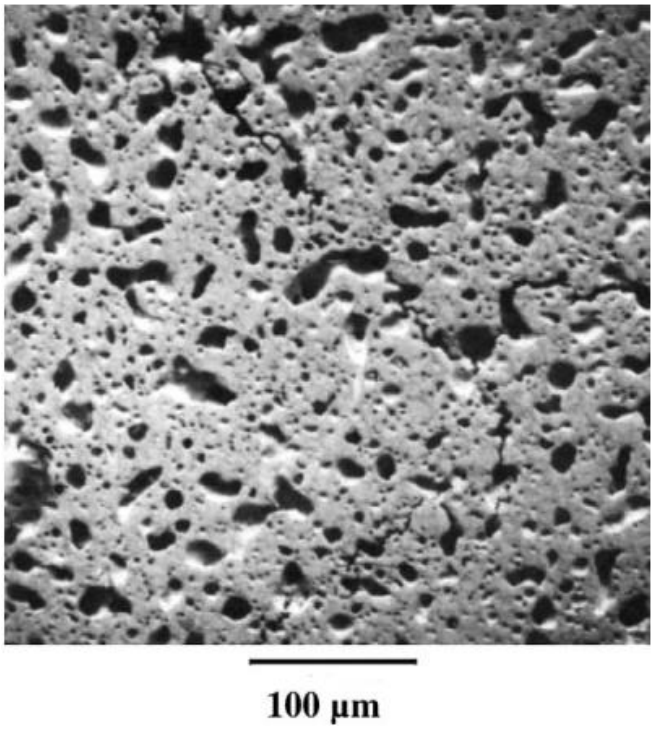

Figure 2. Fission gas pore morphology in irradiated U-10Zr, from [3].

Theoretical work showed that once the swelling reached 30%, the bubbles in the fuel began to interconnect [4]. These interconnections create pathways for the fission gasses to be released to the gas plenum, allowing for the stress on the cladding to remain low [5]. After this critical design adjustment was made, the fuel behaved predictably. This interconnection is visible in Figure 2, and the resulting path for fission gas release is illustrated in Figure 3. As predicted, a smear density of 75% allows the fuel to swell to its maximum extent within the cladding, with further generation of fission gas being accommodated by the gas plenum.

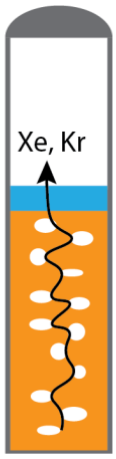

Figure 3. Illustration of interconnected porosity leading to fission gas pathway to gas plenum. Gas travels through pores (white) in the fuel matrix (orange). Note that the fuel has swelled into contact with the cladding, but that the interconnection of gas bubbles reduces the driving force for further swelling.

Due to the gradual interconnection of fission gas bubbles, the release of fission gas to the plenum is not constant. Initially, no fission gas is released, as it stays entirely contained in the bubbles. At ~1 at. %[3] burnup the bubbles begin to interconnect, and the fraction of gas released to the plenum begins to increase, eventually reaching a steady state of ~70-80%, as illustrated in Figure 4 [6]. The high fraction of fission gas release must be accommodated by an appropriately large gas plenum to reduce stress on the cladding from the resulting pressure.

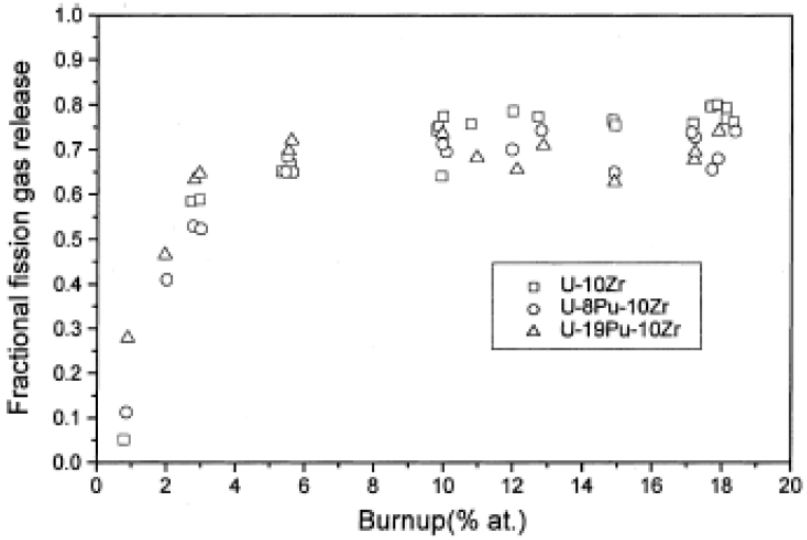

Figure 4. Fission gas release during fuel irradiation tests, adapted from [6].

The swelling behavior of fuel is anisotropic, with proportionately more radial than axial swelling due to temperature gradients in the radial direction, the magnitude of which depends on the core and fuel

[3] Fuel "burnup" is the amount of heavy metal (e.g., uranium, plutonium) that has fissioned. It can be expressed as percent of heavy metal atoms that have fissioned (at. %) or in units of fission energy produced per unit mass of heavy metal (GWd/MTHM or MWd/kgHM). 1 at. % of burnup corresponds to roughly 9.4 GWd/ MTHM [16].

design for a reactor type. Virtually all length increase of the fuel takes place during the burnup interval before the fuel contacts the cladding, which for 75% smear density fuel occurs at ~1 at. % burnup [7]. Axial growth of binary (i.e., U-Zr) fuel is in the range of 8-10%, while ternary (i.e., U-Pu-Zr) fuel is in the range of 3-4% [3]. The anisotropy is particularly pronounced in ternary fuel due to the redistribution of zirconium along the radial temperature gradient (see Constituent Redistribution for more information). Although axial swelling is not typically associated with cladding failure (as is radial swelling), reactor designers must account for it because of its neutronic effects.

Fuel-Cladding Interaction

Fuel-Cladding Mechanical Interaction

If the fuel continues to swell after contacting the cladding, it causes fuel-cladding mechanical interaction (FCMI). This continued swelling puts stress on the cladding and can lead to yielding and cladding breach. FCMI is addressed simply by designing fuel with 75% smear density as described in previous sections of this paper. At this smear density, the swelling of the fuel reaches its maximum as contact with the cladding occurs, resulting in minimal stress on the cladding. FCMI remains minimal as the ductile fuel tends to flow into the open porosity. However, the accumulation of solid fission products will eventually close the open porosity, which will lead to increased FCMI and eventual cladding failure at very high burnup. FCMI can be mitigated by imposing lower burnup limits, which could allow for operation of fuel at higher smear densities so long as swelling is appropriately accounted for by the imposed limit. Proper fuel design therefore effectively eliminates FCMI issues under steady state conditions.

Fuel-Cladding Chemical Interaction

When metal fuel swells during irradiation and contacts the cladding, inter-diffusion of the fuel and the cladding can occur. This inter-diffusion and the associated issues it causes are referred to as fuel-cladding chemical interaction (FCCI). The major issue caused by FCCI is the creation of interaction zones along the inner surface of the cladding that can affect the mechanical integrity of the cladding or contain relatively low-melting phases [8]. This phenomenon is addressed by choosing cladding and fuel alloys that are compatible, setting appropriate temperature limits at the fuel-cladding interface, and limiting burnup.

Predicting FCCI behavior is challenging, because it is a multi-component diffusion problem. For example, with binary fuel and stainless steel there are five major components (iron, nickel, chromium, uranium, zirconium), and many minor components (carbon, nitrogen and oxygen, fission products) [7]. The inter-diffusion of major fuel and cladding components leads to the formation of new phases at the fuel-cladding interface. Therefore, phase diagrams of binary combinations of these components offer useful insight into FCCI. For instance, they include the intermetallic phases present (since they can form during the inter-diffusion process), the solid-solubility ranges in different phase regions (wide solubility in terminal alloys with good contact can indicate that inter-diffusion rates are high), and the temperatures and compositions to develop liquid phases (as relatively low-melting phases may form at the fuel-cladding interface) [8].

Of particular concern is the formation of U-Fe and Pu-Fe, alloys that have lower melting temperatures than the fresh fuel. These lower melting temperatures can reduce margin to fuel melting at steady state conditions or cause melting in off-normal conditions [8]. Typically, these alloys form due to diffusion of iron from the cladding to the fuel, rather than diffusion of the heavy metal (e.g., uranium or plutonium)

to the cladding. As an example, Figure 5 clearly shows that UFe_2 and U_6Fe phases are present in the U-Fe diagram, meaning that these phases could be present in an FCCI zone that develops in irradiated fuel.

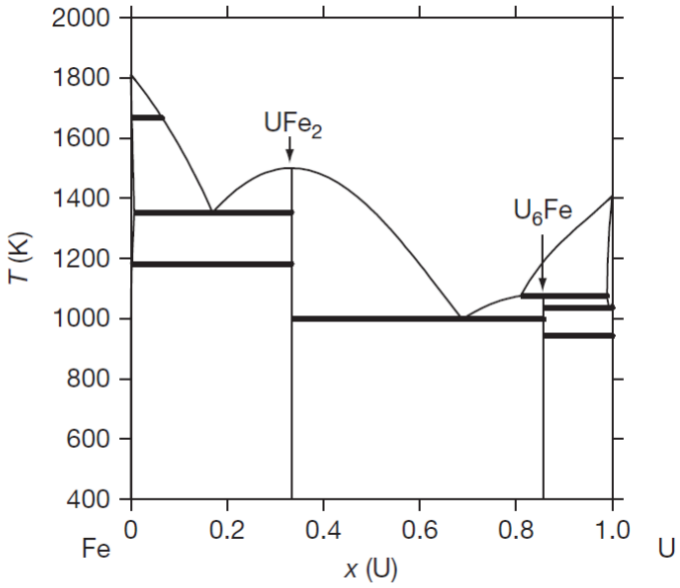

Figure 5. The U-Fe phase diagram, from [9].

Since fission products are generated at increasing concentrations during metal fuel irradiation and can be present at the fuel-cladding interface, phases containing these fission products are also of interest. Specifically, lanthanide fission products have been observed in large concentrations at the fuel-cladding interface and are usually identified as the major cause of FCCI [8].

Both out-of-reactor and in-reactor tests have been performed to better understand FCCI. Out-of-reactor experiments included diffusion couple experiments[4], which provided information about thermal diffusion without contribution from radiation. In addition to testing inter-diffusion behavior at solid state, tests were performed at temperatures where liquid phases can occur. Onset of liquid phase formation was first observed at the 700 ^{o}C range (U-5Fs with SS304 cladding), although that temperature varied slightly depending on fuel and cladding type [10]. The results of these tests showed that impurities in the fuel or cladding alloys may play a role in determining the FCCI behavior in annealed couples. If enough impurities (e.g., C, O, or N) are added to the alloys, then zirconium-rich layers, which are stabilized by the impurities, develop at the fuel-cladding interface and impede the inter-diffusion process [8] [11].

In terms of in-reactor experiments to investigate FCCI, destructive examinations were completed on fuel elements (U-Zr and U-Pu-Zr with HT9, D9, SS316 cladding) from irradiated EBR-II specimens. Fuel cross sections were examined to help characterize FCCI zones and hardness tests were

[4] Diffusion couple experiments are performed by holding solid pieces of pure elements or alloys in close contact and conducting isothermal heat treatments. The goal is to determine the inter-diffusion behavior of the various components at temperatures of interest.

performed. Specifically, the width of the interaction zones, the fuel, fission product, and cladding constituents present in the zones and the mechanical properties of the zones were of interest. Table 1 summarizes key test data, including cladding materials, fuel composition, burnup, and temperature at the fuel-cladding interface.

Table 1. Results from irradiated fuel element examination at EBR-II, adapted from [8].

Fuel element ID	Cladding	Fuel composition (at. %)	Burnup (at. %)	Fuel-cladding temperature at BOL (°C)[i]	Max zone thickness (μm)	Type of analysis	Components originating in the fuel that are found in cladding layers
DP-81	HT9	U-23Zr	5.0	660	70	EPMA[ii]	Ce, Pr, Nd
DP-11	HT9	U-23Zr	10.0	660	90	EPMA	Ce, Pr, Nd, La, Sm, Pd
DP-04	HT9	U-23Zr	10.0	660	90	EPMA	Ce, Pr, Nd, La, Sm, Pd
DP-70[iii]	HT9	U-23Zr	10.0	660	140	EPMA	Ce, Pr, Nd, La, Sm, Pd
DP-75[iii]	HT9	U-23Zr	10.0	660	170	EPMA	Ce, Pr, Nd, La, Sm, Pd
T459	HT9	U-16Pu-23Zr	3.0	Unknown	10	EPMA	Ce, Pr, Nd
DP-16(1)	HT9	U-16Pu-23Zr	9.7	540	40	SEM[iv]	Ce, Nd, La, U, Pu, Pd
DP-16(2)	HT9	U-16Pu-23Zr	10.1	550	40	EPMA	Ce, Nd, Pr, Pu
DP-21	HT9	U-16Pu-23Zr	11.4	Unknown	Unknown	EPMA	Unknown
C709	D9	U-23Zr	9.3	650	111	EPMA	Ce, Nd, La
T225	D9	U-23Zr	10.0	Unknown	25	OM[v]	Unknown
T141	D9	U-23Zr	11.9	Unknown	17	OM	Unknown
T-159	D9	U-16Pu-23Zr	3.0	Unknown	Unknown	EPMA	Ce, Pr, Nd, Pu
Unknown[vi]	D9	U-16Pu-23Zr	6.0	Unknown	75	EPMA	Ce, Pr, Nd, La
T042	D9	U-7Pu-23Zr	6.0	540	20	EPMA	Ce, Pr, Nd, La
T-087	D9	U-16Pu-23Zr	10.0	Unknown	50	EPMA	Ce, Pr, Nd, La, Pu
A-850	D9	U-16Pu-23Zr	10.1	550	100	EPMA	Ce, Nd, La, Pu
T-112	D9	U-16Pu-23Zr	11.9	Unknown	72	EPMA	Unknown
T-106	D9	U-16Pu-23Zr	17.0	Unknown	20	EPMA	Ce, Pr, Nd, La
T341	SS316	U-16Pu-23Zr	0.4	Unknown	Unknown	EPMA	Unknown

i – Temperatures calculated for beginning of life (BOL) using the code LIFE-METAL. ii – Electron probe micro-analysis (EPMA). iii – DP-70 and DP-75 were fuel elements run in the reactor beyond cladding breach. iv – Scanning electron microscope (SEM). v – Optical microscopy (OM). vi – Label for this element was not found.

These in-reactor experiments determined that the lowest temperature at the fuel-cladding interface was 540^{o}C and the highest was 660^{o}C. The thickest interaction zone measured 170µm, where the lanthanide fission products were the primary fuel constituents observed in the interaction zones. Both temperature and power variations along the length of the fuel appeared to impact of FCCI, with the maximum FCCI being observed in a combined high-temperature and high-power region of the fuel. This region of the fuel has higher inter-diffusion kinetics and the supply of fission products at the fuel-cladding interface is relatively higher.

In addition to temperature and power, burnup was also determined to impact FCCI, where higher burnup fuel elements contained larger interaction zones. This phenomenon is mostly due to the higher concentration of lanthanides, increasing the inventory of fission products at the fuel-cladding interface. In addition, higher burnup fuel spends longer times at higher temperatures, allowing for more time for inter-diffusion of the fuel and cladding [8].

Interaction zone formation is localized, as shown in Figure *6*, and can be attributed to the integrity of the zirconium-rich zone between the fuel and the cladding. This zone seems to be an impurity-stabilizer and does not interact much with the fuel or the cladding. It generally remains stable during irradiation, although it can develop cracks. Although some of the thickest interaction zones are observed where this zirconium-rich zone fails, it is likely to stay intact at lower temperatures and lower power [8].

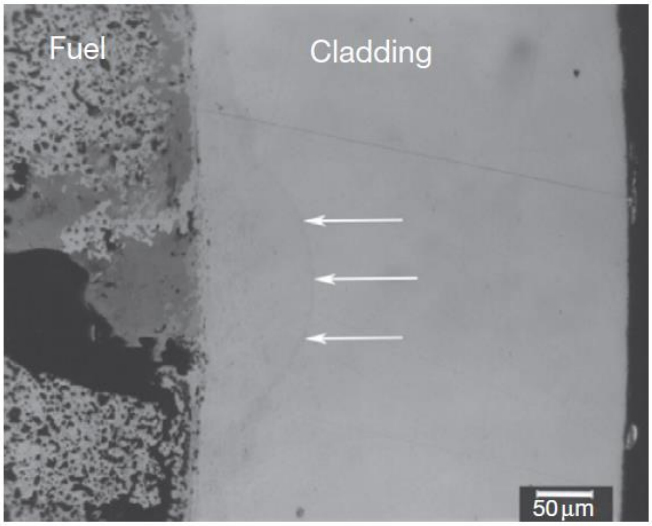

Figure 6. Optical micrograph showing fuel-cladding interaction (white arrows) adjacent to a large deposit of lanthanide fission products, from [8].

Constituent Redistribution

Constituent redistribution refers to the transition from a uniformly mixed fuel alloy to an inhomogeneous mixture during irradiation. It is a diffusion phenomenon, driven by temperature gradients and enhanced by irradiation and phase transformation [12]. Diffusion of the constituent elements creates variations in local composition that increase with time, temperature, and burnup. These variations result in phase transformations, and localized changes in fuel properties such as melting temperature. Redistribution can therefore cause challenges to continued operation, for example by reducing margins to fuel melting. These challenges can be managed by following appropriate time, temperature, and burnup limits, and building in margin to account for the expected changes in fuel properties over fuel lifetime.

Because diffusion is driven by temperature gradients, redistribution primarily occurs radially in the fuel. Figure 7 shows an optical micrograph of redistribution in a ternary fuel element cross section, overlaid with the measured radial composition of each element, from electron probe microanalysis [12]. The redistribution observed here is typical of cylindrical fuel elements, forming distinct radial zones of different composition. Also visible in Figure 7 are the differences in structure of the zones, including pore morphology and relative density. The boundaries between these radial zones correspond to fuel temperatures at which phase changes occur (600 °C and 650 °C for ternary fuel), and the formation of zones depends strongly on the temperature distribution across the fuel [12]. For example, in fuel with lower peak centerline temperatures (below 650 °C) only two zones are observed. Binary fuel typically exhibits very similar redistribution behavior to that shown in Figure 7, with the main difference being that zirconium enriches only in the center, not in the periphery.

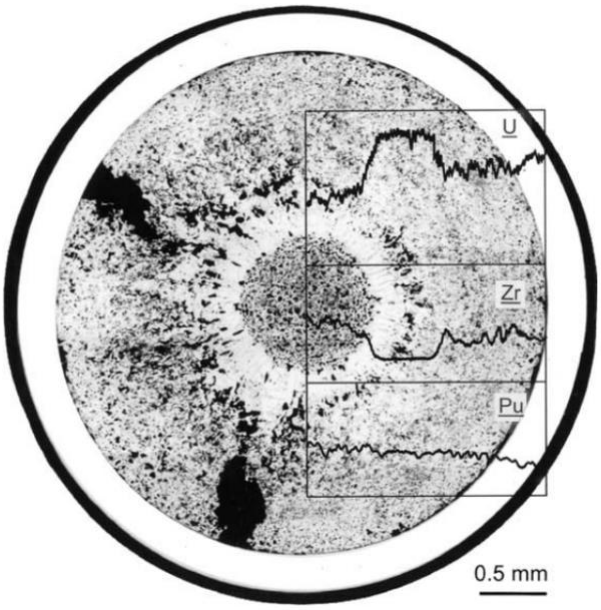

Figure 7. Optical metallography of U-Pu-Zr fuel pin (from an EBR-II fuel element at 1.9 at. % burnup) cross section, and corresponding constituent concentrations measured with electron probe microanalysis, from [12].

Importantly, constituent redistribution plays a key role in other fuel behavior characteristics such as swelling and fuel-cladding interaction mechanisms. Fuel swelling is inherently dependent on phase, and the phase transformations caused by redistribution result in different swelling behavior throughout the

cross-section [13]. This is a key factor in the anisotropy of fuel swelling, in which radial swelling is proportionally much greater than axial swelling (see Fission Gas Release and Fuel Swelling for more information). Similarly, FCCI is inherently dependent on the relative concentrations of constituent materials at the cladding and fuel interface. Because constituent redistribution drives changes in these concentrations over the course of fuel life, it can change the FCCI behavior over time. In some cases, these changes can be beneficial, such as the increase in zirconium concentration at the fuel periphery in ternary fuel [12]. In other cases they can be detrimental, such as the buildup of lanthanides at the fuel-cladding interface at high burnup [8]. Metal fuel designers must critically evaluate the expected changes in their fuel due to redistribution and set the correct operating limits and margins to avoid detrimental effects. For example, by operating at low temperatures and setting low burnup limits, the main driving forces can be removed.

OPERATING EXPERIENCE

Design and Evolution of Metal Fuel

The longest continuous operation of metal fuel in the U.S. was at EBR-II. EBR-II contained driver fuel (i.e., fuel used to drive the fission process) and experimental fuel assemblies. Although many fuel forms were tested over the 30-year operating history of EBR-II, the driver fuel remained metal. The specific form of the driver fuel evolved over time, from initial loadings of U-5Fs to a later conversion to U-10Zr. Nominal design parameters are shown in in Table 2.

Table 2. Nominal design parameters of EBR-II driver fuel, adapted from [14].

	Mark-IA	Mark-II	Mark-IIC	Mark-IICS	Mark-III	Mark-IIIA	Mark-IV
Fuel alloy (wt%)	U-5Fs	U-5Fs	U-10Zr	U-10Zr	U-10Zr	U-10Zr	U-10Zr
Enrichment weight (%^{235}U)	52	67	78	78	66.9	66.9	69.6
Fuel-slug mass (g)	64	52	47	47	83	83	78
Fuel smear density (%)	85	75	75	75	75	75	75
Cladding wall thickness (cm)	0.023	0.030	0.030	0.030	0.038	0.038	0.046
Cladding outer diameter (cm)	0.442	0.442	0.442	0.442	0.584	0.584	0.584
Length (cm)	46.0	61.2	63.0	53.6	74.9	74.9	74.9
Cladding	SS304L	SS316	SS316	SS316	CW[i] D9	CW SS316	HT9
Spacer wire diameter (cm)	0.124	0.124	0.124	0.124	0.107	0.107	0.107
Burnup limit (at. %)	2.6	8	8.9	6.4	10	10	N/A[ii]
Plenum/fuel vol. ratio	0.18	0.83	1.01	0.68	1.45	1.45	1.45

i – Cold worked (CW)
ii – Mark-IV fuel test were not carried to the point of an approved burnup limit.

The early metal fuels used at EBR-II had issues achieving desired burnup requirements for fast-spectrum reactor applications. Swelling of the fuel under irradiation and buildup of fission gas both induced stress on the cladding and limited Mark-I fuel to just 1.2 at. % burnup, and Mark I-A fuel to 2.6 at. % [15]. These design challenges were addressed in the Mark-II fuel that included (1) the addition of impurity-level amounts of silicon to ameliorate the fuel swell rate, (2) a lower smear density to accommodate fuel swell, (3) a larger fuel rod plenum to accommodate released fission gas, and (4) a thicker cladding wall (see Fission Gas Release and Fuel Swelling for more information) [16].

In its final decade of operation, from 1984 to 1994, a transition was made at EBR-II to a new fuel alloy system, with zirconium replacing fissium as the alloying element for the Mark-III, -IIIA and –IV

designs. Zirconium was used to improve compatibility with cladding and increase the fuel melting temperature which mitigates fuel-cladding eutectic formation (see Fuel-Cladding Chemical Interaction for more information) [1] [16].

Transient/Off Normal

EBR-II and the Transient Reactor Test Facility (TREAT) carried out transient tests on metal fuel. The primary difference between these two facilities was the rate of reactivity insertion and subsequent loss of cladding integrity: the transient tests at EBR-II were characterized as slow, whereas the transient tests at TREAT were characterized by more rapid reactivity insertions.

Metal fuel has demonstrated excellent behavior during transients throughout the metal fuel testing program at EBR-II. It is extremely robust, as demonstrated by the sample history of a typical driver fuel pin irradiated during the EBR-II inherent passive safety tests in 1986, shown in Table 3 [1].

Table 3. Sample history of a typical driver fuel pin during EBR-II inherent passive safety tests in 1986, from [1].

Number of transients	Description
40	start-ups and shutdowns
5	15% overpower transients
3	60% overpower transients
45	loss-of-flow (LOF) and loss-of-heat-sink tests including a LOF from 100% power without scram

Operational Reliability Tests

Although the operational reliability tests (ORT) were carried out on experimental fuel at EBR-II, the effects on the Mark-II driver fuel were also analyzed to further understand and qualify the metal fuel for transient conditions. These tests were performed on U-Fs driver fuel, and the results were also extended[5] to U-Zr driver fuel. The program consisted of out-of-reactor and in-reactor testing and two reactivity ramp rates were considered: 1.6%/second (56 tests) and 4MW/second (13 tests). No indication of cladding breaches nor performance degradation was found of the driver fuel through simple surveillance of the core after the low-ramp-rate tests. The examination for the high-ramp-rate test was more detailed, investigating five test assemblies that contained driver fuel that had experienced the low-ramp-rate tests prior to the high-ramp-rate tests (burnup 0-10 at. %). Nevertheless, the test program showed that this metal driver fuel, which included assemblies that were operating at the upper boundaries of expected temperature, withstood the transient tests with no apparent damage [16].

[5] Results of test programs carried out on earlier fuel designs were easily "extended" to U-Zr and U-Pu-Zr fuels. This was possible because the phenomena known to control metal fuel lifetime (e.g., swelling, fission gas release, fuel-cladding interaction) were found to be either comparable or less limiting in U-Zr and U-Pu-Zr fuels than those observed in the U-Fs fuel, which had formed the bulk of the metal fuel database [16]. Effectively this meant that the results were assumed to be representative for the later designs without the need to conduct new tests for each iteration of fuel.

Performance

More than 130,000[6] metal fuel elements were irradiated during the lifetime of EBR-II, and the irradiation history is a testament to the continuous effort that was made to improve performance. Additionally, over 1,000 U-Zr and U-Pu-Zr fuel rods were irradiated at the Fast Flux Test Facility (FFTF) [17]. As performance limits were reached for a given iteration of fuel, adjustments were made to eliminate or extend that limit and each successive generation of fuel operated longer and more reliably. At the end of this paper, Table 6 shows a summary of selected metal fuel irradiation experiments at EBR-II and FFTF.

One of the most often cited concerns regarding the EBR-II fuel irradiation tests, which were performed on a small core (i.e., the fuel rods were 34.3 cm in length), was that the behavior of these short rods might not be representative of that of longer rods [1]. There was a belief that fuel columns on the order of 1 m long, as were expected in future commercial reactors, could slump under their own weight during irradiation [18]. Testing at FFTF resolved this widely-spread concern.

Over 800 HT9-clad U-10Zr fuel elements, 91.4 cm tall, were irradiated at FFTF as part of a planned conversion of the FFTF core from oxide to metal fuel [19]. Burnups of up to 14 at. % were reached, with peak cladding temperatures up to 651 °C, without cladding breach or fuel slumping issues. A smaller number of ternary U-Pu-Zr fuel were also tested up to 9% burnup. Further, the post-irradiation examination of these experiments showed that the fission gas release, constituent migration, and axial growth were as predicted, with no significant deviations from previous experience with shorter rods [1].

Cladding Breach

Cladding breach is penetration of the cladding, which serves as the boundary between the fuel and the coolant and is considered the first fission product barrier. In early metal fuel designs (Mark I,-IA) used at EBR-II, cladding breach was caused by FCMI from fuel swelling at burnups of 1-3 at. % [15]. In the subsequent Mark-II design, the smear density was lowered to 75% to accommodate swelling, effectively eliminating failures due to FCMI (see Fission Gas Release and Fuel Swelling, Fuel-Cladding Mechanical Interaction for more information). Following this critical change, very few elements experienced cladding breach and much higher burnups were routinely achieved. Specifically, cladding breach did not occur in Mark-II fuel until 10 at. % [5]. Ultimately the burnup limit would likely have achieved 15 at.% or better with MK-IIA fuel. The biggest remaining challenge to the cladding was the stress caused by fission gas pressure, which increases with burnup and must be accommodated in the fission gas plenum.

As EBR-II transitioned from Mark-II fuel, evidence of the substantial improvements was seen in the outstanding performance of the Mark-III/-IIIA/-IV fuel. Out of the 16,811 U-Zr and 660 U-Pu-Zr fuel elements that were irradiated at EBR-II, only 22 experienced cladding breach [20]. Defective welds were the cause of breach in 16 of the 22 fuel elements, an issue that was eradicated early in the program. Three cladding breaches occurred in the plenum region due to unknown causes [16]. After these breaches, metal fuel designs were modified to incorporate a larger fission gas plenum, with a plenum to fuel volume ratio of 1.4 becoming the reference for EBR-II experiments and driver fuel [16]. Lastly, three fuel elements breached in the fuel column region due to creep failure [20]. One of these fuel column failures occurred in fuel that reached very high burnup (16.4 at. %) [16]. The other

[6] Of the 130,000+ metal fuel pins that were irradiated at EBR-II, about 90,000 were Mark-I/-IA driver fuel pins, over 30,000 were Mark-II driver fuel pins, and more than 16,000 were Mark-III/-IIIA/-IV driver fuel pins [16].

two occurred at 9.5 at. % burnup in elements that were intentionally operated at higher than normal temperatures (660 ^{o}C for HT9 cladding) [21].

These 22 breaches led to appropriate fuel design changes and improvements in fabrication. The small number of failures, and the constant push to improve the fuel designs in response, have effectively made cladding breach a concern only under particularly challenging temperature regimes or at very high burnups.

Run Beyond Cladding Breach Tests

While very few elements breached during normal operation, an important goal of the metal fuel testing program at EBR-II was to understand the operational behavior of the fuel with breached cladding, called run beyond cladding breach (RBCB) scenarios. Since the major concerns regarding RBCB were the compatibility of the coolant with the fuel and the escape of the fuel or fission products to the coolant, several fuel elements were intentionally breached for observation. Some elements were irradiated to their natural breach occurrence, and others were machined to contain defects. These elements were re-inserted into the reactor where they were intended to breach [16]. A summary of the seven intentionally breached rods and naturally breached rods are shown in Table 4.

Table 4. Summary of RBCB experiments at EBRI-II, adapted from [16].

Test ID	Test type	No. of rods	Fuel composition	Cladding type	Cladding OD (cm)	Pitch-to-diameter ratio	Linear power[i] (kW/m)	Cladding temp. (°C)	Burnup[ii] (at. %)	Rods breached	Time irrad. post breach (days)
XY-21	BFTF[iii]	1, 60[iv]	U–5Fs	SS316	0.44	1.38	24	573	7.9	0	N/A
XY-21A	BFTF	1, 60 iv	U–5Fs	SS316	0.44	1.38	25	593	9.3	1	54
XY-24	FPTF[v]	2, 59 iv	U–19Pu–10Zr	SS316	0.44	1.38	21	541	7.6	1	233
XY-27	BFTF	2, 59 iv	U–8Pu–10Zr	SS316	0.44	1.38	23	520	~6.0	2	131
X482	Open core	1, 60 iv	U–19Pu–10Zr	D9	0.58	1.24	39	600	14.4	1	168
X482A	Open core	1, 60 iv	U–10Zr	D9	0.58	1.24	36	600	13.5	1	100
X482B	Open core	1, 60 iv	U-19Pu-10Zr	HT9	0.58	1.24	36	600	~14	1	150
X420B	Natural breach	61	U-19Pu-10Zr	D9	0.58	1.24	--	--	~17	1	34

i – Linear power values are pre-test predictions.
ii – Burnup values are burnup at end of test.
iii – Breached Fuel Test Facility (BFTF) at EBR-II provided separate delayed neutron signal monitoring for the experiment and an above-core sampler for collection of released fuel and contamination.

iv – First number indicates the number of pre-defected (thinned) rods, and the second number indicates the remaining number of rods in the assembly. Note that the XY-series tests used instrumented assemblies that contained 61 Mark-II-size EBR-II rods, which would typically fill a 91-pin EBR-II Mark-II driver assembly.
v – Fission Product Test Facility (FPTF) at EBR-II had the capability for monitoring fission products released from a breached fuel rod.

The resulting behavior from the breached rods showed that metal fuel is chemically compatible with sodium coolant, since there were no fuel-coolant reaction products, nor substantial washing out of fuel into the coolant. Breaches were not substantially widened, because the breach released any pressure from fission gas. Bond sodium, fission gas, and cesium were released to the coolant, but overall it was determined that a sodium fast reactor could operate benignly with breached fuel. This meant that the breach of a single metal fuel element would not necessarily require shutdown, and the reactor could continue to operate until a convenient time, or even the end of the cycle, prior to replacing the breached element. Examples of metal and oxide breached elements are shown in Figure 8, and the weakness and failure location are clearly visible. The cross section of the oxide fuel pin shows the vastly different behavior, in which the initial breach site is widened and fuel is lost to the sodium coolant.

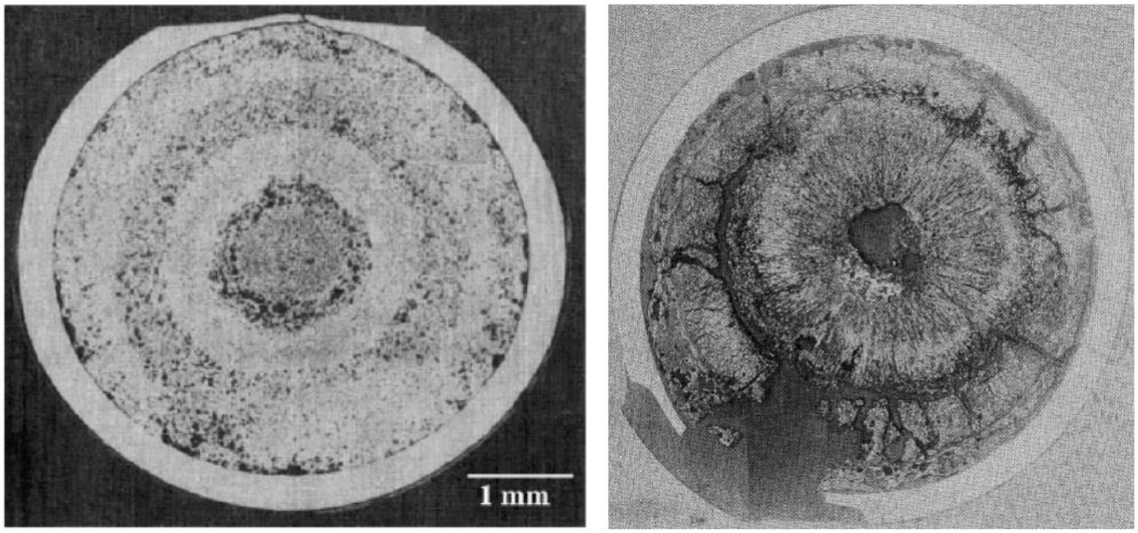

Figure 8. Example of RBCB test of 12 at. % metal (left) and 9 at. % oxide (right) fuel element, from [20]. Note that the metal fuel displays no reaction products and no noticeable fuel loss to the sodium coolant, while the oxide fuel shows signs of widened breach site, sodium-fuel interaction products, and fuel loss.

Shutdown Heat Removal Tests

As the IFR development program progressed, the IFR safety program also conducted a series of passive safety tests at EBR-II, known as shutdown heat removal test (SHRT) program. The program successfully demonstrated the ability of a metal-fueled fast reactor to withstand loss-of-flow-without-scram (LOFWS) and loss-of-heat-sink-without-scram (LOHSWS) with no core damage and no adverse effects on operation [22] [23]. Both experiments took place on the same day (April 3, 1986). Similarly to ORT, this aggressive test program was necessary to address the damage to the EBR-II driver fuel and to help qualify the fuel for transient operation. The cladding damage analysis showed (1) incremental damage to the fuel as low and (2) high probability that the driver fuel would reach its burnup limit. Although the examined fuel for these tests was U-Fs, the results were extended to U-Zr [16].

The LOFWS event simulates a scenario in which all sources of power are lost, and all methods of shutting down the reactor fail. In the unlikely event that each of these redundant systems fail, the primary pump loses power, and coolant flow is rapidly reduced while the reactor remains at full power. In the LOFWS testing conducted at EBR-II, the coolant outlet temperature rose very rapidly, as shown in Figure 9. This rapid rise, 200 °C in 30 seconds, caused core components including fuel and structures to heat up and thermally expand, enhancing neutron leakage and introducing a large negative reactivity feedback that shut down the reactor. The temperature then returned to equilibrium. Figure 9 shows the excellent agreement between the predicted and actual behavior during the test.

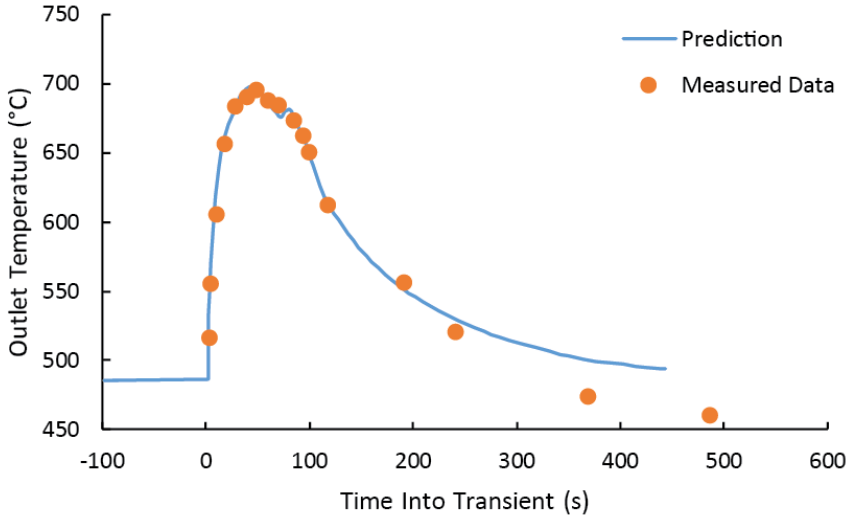

Figure 9. LOFWS outlet temperature vs. time, comparing predicted and measured data. The initial spike in temperature causes negative reactivity feedback that shuts the reactor down, and the temperature returns to steady state. Adapted from [24].

The LOHSWS, conducted later the same day, simulated the loss of heat sink by shutting down the intermediate pump, thereby isolating the primary system. The primary loop continued to remove heat from the core, but the heat was dumped entirely to the primary sodium, raising the core inlet temperature. The transient was slower, raising the primary sodium temperature 40 °C in 10 minutes, but the result was the same: power was reduced and the reactor shut down due to thermal expansion and enhanced neutron leakage. Figure 10 shows that the initial spike in reactor inlet temperature creates a corresponding reduction in power level, shutting down the reactor, and the gradual equalization of reactor inlet and outlet temperatures confirms that the power level has essentially dropped to zero.

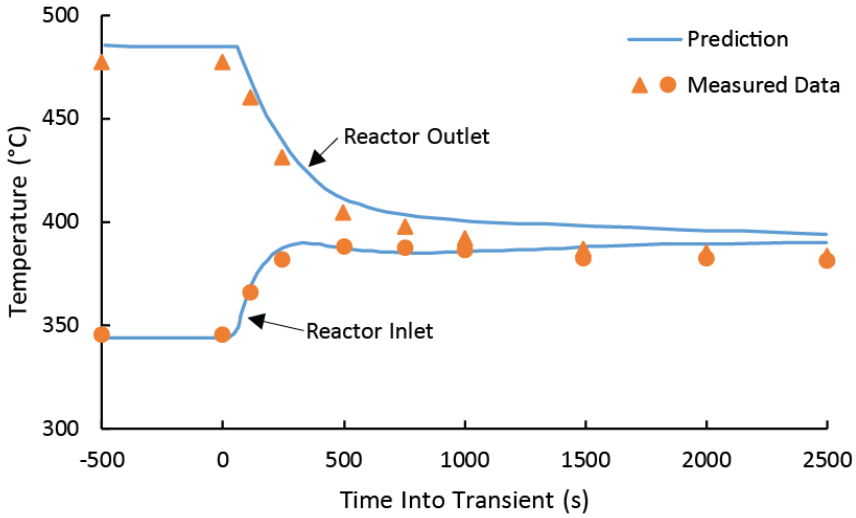

Figure 10. LOHWS inlet and outlet temperatures vs. time, comparing predicted and measured data. The initial spike in inlet temperature causes negative reactivity feedback, which reduces power and correspondingly reduces the reactor outlet temperature. Adapted from [24].

The results of these two tests demonstrated the unique inherent safety characteristics of both liquid sodium cooled reactors and metal fuel. The large thermal inertia of the sodium tank and the large margin to boiling of sodium both allowed for the reactor structures to heat up and introduce sufficient negative reactivity to safely shut down prior to boiling of the sodium. No appreciable fuel damage occurred, no radioactive particles were released, and the reactor was restarted after the tests later the same day. Thus, two accidents that are typically highly-challenging to LWRs, posed no safety threat to EBR-II.

Transient Overpower Tests

Various combinations of fuel and cladding alloys were evaluated at TREAT to determine transient-overpower margin to failure, pre-failure axial fuel expansion, and post-failure fuel and coolant behavior. These tests were conducted on 15 pins of various combinations of fuel (U-Fs, U-Zr, U-Pu-Zr) with cladding (SS316, D9, HT9) as summarized in Table 5. In these tests, the metal fuel failed at 4-4.5 times nominal peak power under the relatively fast transient conditions used in the tests [3] [25]. Conversely, oxide fuel tested under the same conditions failed at just 2.5-3 times nominal peak power, demonstrating the larger margin to cladding failure for metal fuel.

Table 5. Summary of selected TREAT experiments, adapted from [16].

Test ID	Fuel/cladding	Burnup (at. %)	Transient rate	Overpower attained in test $(P/P_0)^i$	Calculated breach threshold	Comments
M2	U–5Fs/SS316; Mark-II design	0.3	8-s period	4.1	4.7	16% max. axial expansion; fuel damaged but intact

	U–5Fs/SS316; Mark-II design	4.4	8-s period	4.2	4.5	Cladding breached
	U–5Fs/SS316; Mark-II design	7.9	8-s period	4.1	3.6–4.0	3% max. axial expansion; cladding breached
M3	U–5Fs/SS316; Mark-II design	0.3	8-s period	4.1	4.8	18% max. axial expansion; fuel damaged but intact
	U–5Fs/SS316; Mark-II design	4.4	8-s period	4.0	4.4	4% max. axial expansion; fuel damaged but intact
	U–5Fs/SS316; Mark-II design	7.9	8-s period	3.4	3.6–4.0	4% max. axial expansion; fuel damaged but intact
M4	U–5Fs/SS316; Mark-II design	0.0	8-s period	3.8	4.3	4% max. axial expansion; fuel damaged but intact
	U–5Fs/SS316; Mark-II design	2.4	8-s period	4.1	4.4	7% max. axial expansion; cladding breached
	U–5Fs/SS316; Mark-II design	4.4	8-s period	3.8	4.3	4% max. axial expansion; fuel damaged but intact
M5	U–19Pu–10Zr/D9; X419,420,421 design	0.8	8-s period	4.3	5.1	1% max. axial expansion; fuel damaged but intact
	U–19Pu–10Zr/D9; X419,420,421 design	1.9	8-s period	4.3	5.1	2% max. axial expansion; fuel damaged but intact
M6	U–19Pu–10Zr/D9; X419,420,421 design	1.9	8-s period	4.4	4.6	2–3% max. axial expansion; fuel damaged but intact
	U–19Pu–10Zr/D9; X419,420,421 design	5.3	8-s period	4.4	4.5	3% max. axial expansion; cladding breached
M7	U–19Pu–10Zr/D9; X419,420,421 design	9.8	8-s period	4.0	4.4	3% max. axial expansion; cladding breached
	U–10Zr/D9; X425 design	2.9	8-s period	4.8	4.4	2–4% max. axial expansion; fuel damaged but intact
i – The overpower value is reported as peak linear power attained in TREAT test relative to nominal power typical of fast reactor application (~40 kW/m).						

All fuel rod breaches in the metal fuel were located at the top of the fuel column and were due to cladding rupture induced by at-temperature pin-plenum pressure and cladding thinning due to eutectic-like formation of a molten fuel/cladding phase that penetrated the cladding wall. Axial fuel expansion

that occurs pre-failure has the benefit of adding negative reactivity to the core during an overpower transient for the zirconium-alloyed fuels (similar effects were observed with higher-burnup U-Fs fuel); this effect has no parallel in oxide fuel [1]. Rapid fuel dispersal (i.e., half of fuel inventory being ejected from the fuel rod) that occurred post-failure was also found to beneficially add negative reactivity to the core [16].

Fabrication

Metal fuel can be fabricated using a variety of methods. To be practical for mass production, the process should be cost efficient and minimize radioactive waste. Depending on the application, other criteria have increased importance. For example, if recycling spent fuel, the process should be suitable for remote operation in a hot cell. Injection casting meets this requirement, and was therefore used at EBR-II, becoming the most established fabrication method. Other fabrication methods include centrifugal casting, continuous casting, gravity casting, atomizing, and extrusion.

As with any fabrication method, the injection casting parameters must be carefully controlled to prevent defects, but these parameters are well understood. Fuel for EBR-II was cast on site at the EBR-II Fuel Cycle Facility, as well as by Aerojet Nuclear and Atomics International, both of which fabricated 24,000 metal fuel elements for the reactor [26]. In addition to the substantial experience at EBR-II, the Central Research Institute of Electric Power Industry (CRIEPI) built and operated engineering-scale injection casting equipment and reported the successful fabrication of U-Zr fuel pins in 2007 [27]. The substantial experience base and demonstrated repeatability of injection casting makes it a strong candidate for future metal fuel fabrication. The main disadvantage of injection casting is that the silica molds must be broken to remove the fuel and are not reusable, creating an undesirable radioactive waste stream [28].

Other casting methods have been used, and continue to be investigated. Centrifugal casting, in which the melt is injected by centrifugal force, was used for EBR-I fuel slugs [28]. The main concerns with this method are a relatively low throughput and complicated equipment. Gravity casting has also been investigated, in which the fuel melt is poured into molds (with or without assistance of pressure difference). Gravity casting does not require evacuating the furnace, which is beneficial when processing spent fuel because it suppresses the evaporation of americium, a major challenge to other casting methods [29]. INL is developing an advanced casting system utilizing gravity casting and experimenting with re-usable molds, which would be an improvement over the one-time use silica molds in injection casting [30]. Continuous casting eliminates molds altogether and has been successfully demonstrated for U-Zr fuels [31]. The major challenge for continuous casting is that it requires fairly complex equipment and careful alignment; all of which must be automated if throughput is to be sufficient for industrial scale production.

Alternatives to casting have also been investigated. Fabrication of particulate metal fuel by atomization has been studied by a number of groups in Japan, Korea, and the United States [32] [33] [34]. Fuel particles can be fabricated by gas atomization or centrifugal atomization and range in diameter from tens to hundreds of microns. By combining fuel particles of two different diameters, the filling fraction (or effective smear density) can be tuned, for instance to 75%. The key advantage of particulate fuel is that this low filling fraction approximates already-swelled fuel, which can contact the cladding from beginning of operation without a need for sodium bond, and limited swelling due to pre-existing fission gas release pathways. This method also has potential for higher throughput than casting methods and the ability to create unique shapes much more easily. It can be introduced directly into the cladding

without the need for a mold, and sintered in place [35]. Extrusion of fuel elements has also been demonstrated on a lab scale at INL, with ongoing testing underway.

The wide variety of fabrication methods available for metal fuel provide flexibility to design the appropriate process for a given application. Some methods, such as injection casting, do not require additional finishing steps and are therefore well suited for automated processing in a hot cell [1]. For methods that do require additional finishing, metal is amenable to a wide range of well-established techniques. For example, controlled heat treatment can be used to remedy unfavorable textures introduced during fabrication [26]. Advanced manufacturing techniques, such as electrical discharge machining [36], can be used to create very fine surface finish, or to machine complicated shapes for unique fuel geometries. Metal fuel is also robust against defects, demonstrated by the fact that cracks formed during irradiation tend to be filled by the continued swelling of the fuel [1]. Metal fuel offers many advantages in fast reactors, and the relative ease and flexibility of manufacturing serves to extend these benefits to a wide range of potential fuel forms.

Analytical Tools

U.S. national laboratories continue work on higher fidelity computer codes to improve upon the legacy codes to perform metal fuel performance analysis. These efforts are made easier due to the reduced amount of physical effects that metal fuel experiences during irradiation as compared to oxide fuel.

BISON is a high-fidelity tool developed at the Idaho National Laboratory (initially released in 2013) that uses the finite-element method to solve the partial differential equations for material stress-strain and heat conduction, as well as species diffusion. BISON can model generic, complex geometries: virtually anything that can be constructed in computer-aided design software can be simulated. This flexibility in geometry modeling capability makes BISON a powerful tool in analyzing the performance of metal fuel for a wide range of advanced reactor designs. BISON incorporates models for swelling due to fission gas production and associated materials property modifications that occur during irradiation, in both the fuel and the cladding. Some of these BISON models are taken from legacy metal fuel performance codes such as LIFE-METAL [37].

LIFE-METAL (and related tools developed by ANL such as FPIN2 and DEFORM5) use mechanistic models and experimental data from the EBR-II and the IFR programs to characterize metal fuel performance in the traditional cylindrical pin configuration. These tools can still serve as a useful supplement for metal fuel performance analyses since their capabilities have been validated against historical data and their methods of solution are faster than the finite-element approach used by BISON [38]. However, since their method of solution is limited to the very specific cylindrical pin geometries employed by sodium fast reactors such as EBR-II and the proposed IFR, BISON is better suited for explicitly modeling alternative geometries that differ significantly from the traditional pin-type layout.

The ANL systems-level safety analysis tool, SAS4A/SASSYS, incorporates some of these mechanistic fuel performance models to characterize the behavior of the fuel during various potential reactor transients. SAS4A/SASSYS were initially developed during the EBR-II and IFR programs, but have been continually supported since their initial release. The safety analysis simulations generated using SAS4A/SASYS have been validated using data from the EBR-II ORT and SHRT tests, among others. While SAS4A/SASSYS is currently limited to modeling the behavior of sodium-cooled fast reactors with pin-type

fuel (metal or oxide), its capabilities could be extended to a wider range of reactor types in the future [39].

Table Summary of EBRI-II and FFTF Irradiation Experiments

Table 6. Summary of selected metal fuel irradiation experiments in EBR-II and FFTF, adapted from [16].

Experiment number	Fuel composition	Cladding material	No. of rods in assembly	Smear density (%)	Cladding outer diameter (cm)	Wall thickness (cm)	Plenum/fuel vol. ratio	Peak power (kW/m) (BOL)	Peak cladding temp (°C) (BOL)	Peak burnup (at. %)	Fast fluence 10 * 22 n/cm2 (E > 0.1 MeV)	Key rod info.
X419 Prototype and fuel behavior	U-10Zr, U–8Pu–10Zr, U–19Pu–10Zr	D9	61	75	0.584	0.038	1	39.4	560	11.9	12	
X420 Prototype, fuel behavior, failure mode, RBCB	U–10Zr, U–8Pu–10Zr, U–19Pu–10Zr	D9	61	75	0.584	0.038	1	36.1	590	18.4	18.5	1 breach at 16.4 at. % burnup and 530 °C
X421 Prototype, fuel behavior, failure mode	U–10Zr, U–8Pu–10Zr, U–19Pu–10Zr	D9	61	75	0.584	0.038	1	39.4	560	17.1	19.6	
X423 Fuel swelling and restructuring	U–10Zr, U–3Pu–10Zr, U–8Pu–10Zr, U–19Pu–10Zr, U–22Pu–10Zr, U–26Pu–10Zr	SS316	37	75	0.737		1	42.7	522	4.9	8.07	

X425 (X425A/B/C) Lead IFR	U–10Zr, U–8Pu–10Zr, U–19Pu–10Zr	HT9	61	75	0.584	0.038	1	48.2	590	3,11,16.2, 19.3	20.6	
X429 (X429A/B) Fabrication variables and strain prediction	U–10Zr, U–8Pu–10Zr, U–19Pu–10Zr	HT9, SS316	61	75	0.584	0.038	1	42.7	600	7.7, 10.6, 14.4	13.8	1 breach at 6.5 at. % and 1 breach at 10 at. %
X430 (X430A/B) peak cladding temp, large diameter, compatibility	U–10Zr, U–19Pu–10Zr, U–22Pu–10Zr, U–26Pu–10Zr	HT9	37	75	0.737	0.041	1.4	49.2	540	11.5	20.6	
X431 (X431A) Blanket safety	U–2Zr, U–6Zr, U–10Zr	HT9	19	85	0.940	0.038–0.051	1.8	39.4	507	3.9	15.4	
X432 (X432A) Blanket safety	U–2Zr, U–6Zr, U–10Zr	HT9	19	85	0.940	0.038–0.051	1.8	39.4	507	4.5	16.6	
X435 (X435A) Mk-III qual.	U–10Zr	D9	61	75	0.584	0.038	1.4	49.2	591	19.8	22.8	
X436 Mk-III qual.	U–10Zr	D9	61	75	0.584	0.038	1.4	34.4	596		8.45	
X437 Mk-III qual.	U–10Zr	D9	61	75	0.584	0.038	1.4	37.7	597		10	

X438 Mk-III qual.	U–10Zr	D9	61	75	0.584	0.038	1.4	32.8	623		9.45	
X441 (X441A) FCMI test and LIFE-METAL benchmark	U–19Pu–6Zr, U–19Pu–10Zr, U–19Pu–12Zr	HT9, D9	61	70–85	0.584	0.038	1.1–2.1	45.9	600	12.7	10.1	
X447 (X447A) U–Zr high temp.	U–10Zr	HT9	49	75	0.584	0.046	1.4	36.1	660	10	9.17	
X448 (X448A) Mk-IV qual.	U–10Zr	HT9	61	75	0.584	0.046	1.4	45.9	552	14.6	14.9	
X449 Mk-IV qual.	U–10Zr	HT9	61	75	0.584	0.046	1.4	29.5	578	11.3	17.7	
X450 Mk-IV qual.		HT9	61	75	0.584	0.046	1.4	36.1	576	10.2	13.1	
X451 (X451A) Mk-IV qual.	U–10Zr	HT9	61	75	0.584	0.046	1.4	32.8	623	13.7	13.7	
X452 Fuel impurities	U–10Zr	D9	61	75	0.584	0.038		34.4	596	6.1	5.38	
X453 Fuel impurities	U–10Zr	D9	61	75	0.584	0.038		34.4	596	8.5	8.45	
X454 Fuel impurities	U–10Zr	D9	61	75	0.584	0.038		49.2	547	8.3	9.12	
X455 Fuel impurities	U–10Zr	D9	61	75	0.584	0.038	1.4	49.2	547	10.3	9.16	
X481 Mk-III design with Pu	U–19Pu–10Zr	D9	61	75	0.584	0.038	1.4	49.2	579	10	11.3	

X483 (X483A) Mk-IIIA, ref. SS316 qual.	U-10Zr	SS316	61	75	0.584	0.038	1.4	49.9	552	14.8	15.7	
X484 Mk-IIIA ref. SS316 qual.	U-10Zr	SS316	61	75	0.584	0.038	1.4	36.1	576	11.7	11.9	
X485 Mk-IIIA ref. SS316 qual.	U–10Zr	SS316	61	75	0.584	0.038	1.4	39.7	576	10.5	10.7	
X486 Mk-IIIA ref. SS316 qual.	U–10Zr	SS316	61	75	0.584	0.038	1.4	37.1	623	13.9	13.9	
X489 High-Pu for PRISM design	U–19Pu–10Zr, U–28Pu–10Zr	HT9, HT9 M[i]	61	75	0.584	0.046	1.4	36.1	606	5.4	4.83	
X492 (X492A/B) Zr-sheathed fuel	U–3Zr, U–20.5Pu–3Zr	HT9, HT9 M	61	75	0.584	0.038	1.4	41.0	551	10.5	11.1	
X496 Long lifetime	U–10Zr	HT9	37	59	0.686	0.056	3	63.3	536	8.3	6.9	
X501 Minor-actinide-bearing fuel	U–20.2Pu–10Zr–1.3Np–1.2Am, U–10Zr	HT9	2 + 59	75	0.584	0.046	1.4	44.9	≤540	7.6	6.4	
IFR-1 Fuel column length effects	U–10Zr, U–8Pu–10Zr U-19Pu-10Zr	D9	169	75	0.686	0.056	1.2	49.2	615(604)	94 GWd/MTHM	15.4	

MFF1A FFTF lead metal fuel test	U–10Zr	HT9	8	75	0.686	0.056	1.2	42.7	577	38 GWd/ MTH M	5.6	
MFF-1 FFTF lead metal fuel test	U–10Zr	HT9	5	75	0.686	0.056	1.2	43.0	577	95 GWd/ MTH M	17.3	
MFF-2 FFTF metal prototype	U–10Zr	HT9	169	75	0.686	0.056	1.3	54.1	618	143 GWd/ MTH M	19.9	
MFF-3 FFTF metal prototype	U-10Zr	HT9	169	75	0.686	0.056	1.3	59.1	643	138 Gwd/ MTH M	19.2	
MFF-4 FFTF series III.b qual.	U–10Zr	HT9	169	75	0.686	0.056	1.5	56.8	618	135 GWd/ MTH M	19	
MFF-5 FFTF series III.b qual.	U–10Zr	HT9	169	75	0.686	0.056	1.5	55.8	651	101 GWd/ MTH M	14	
MFF-6 FFTF series III.b qual.	U–10Zr	HT9	169	75	0.686	0.056	1.5	55.8	588	141 GWd/ MTH M	12.8	
i – HT9M is modified HT9, containing the same elements (C, Si, Mn, Ni, Cr, Mo, V, Nb, W, N) in different compositions than HT9.												

References

[1] Y. Chang, "Technical Rationale for Metal Fuel in Fast Reactors," Argonne National Laboratory, Argonne, 2007.

[2] C. Till and Y. Chang, Plentiful Energy, 2011.

[3] W. Carmack, D. Porter, Y. H. S. Chang, M. Meyer, D. Burkes, C. Lee, T. Mizuno, F. Delage and J. Somers, "Metallic fuels for advanced reactors," *Journal of Nuclear Materials,* vol. 392, pp. 139-150, 2009.

[4] R. Barnes, "A Theory of Swelling and Gas Release for Reactor Materials," *Journal of Nuclear Materials,* pp. 135-148, 1964.

[5] L. Walters, "Thirty years of fuels and materials information from EBR-II," *Journal of Nuclear Materials,* vol. 270, pp. 39-48, 1999.

[6] C. Lee, D. Kim and Y. Jung, "Fission Gas Release and Swelling Model of Metallic Fast Reactor Fuel," *Journal of Nuclear Materials,* vol. 288, pp. 29-42, 2001.

[7] G. Hofman, L. Walters and T. Bauer, "Metallif Fast Reactor Fuels," *Progress in Nuclear Energy,* vol. 31, pp. 83-110, 1997.

[8] D. Keiser, "Metal Fuel-Cladding Interaction," in *Comprehensive Nuclear Materials*, Amsterdam, Elsevier, 2012.

[9] M. Kurata, K. Nakamura and T. Ogata, "Thermodynamic evaluation of quaternary U-Pu-Zr-Fe system-assessment of cladding temperature limits of metallic fuel in a fast reactor," *Journal of Nuclear Materials,* vol. 294, pp. 123-129, 2001.

[10] S. Zegler, H. Rhude and J. Lahti, "Compatibility of Uranium-5 w/o Fissium alloy with types 304L and 316 stainless steel," Argonne National Laboratory, Argonne, 1969.

[11] C. Hofman, A. Hins, D. Porter, L. Leibowitz and E. Wood, "Chemical interaction of metallic fuel with austentic and ferritic stainless steel cladding," in *Reliable fuels for liquid metal reactors*, Tuscon, 1986.

[12] Y. Kim, G. Hofman, S. Hayes and Y. Sohn, "Constituent redistribution in U-Pu-Zr fuel during irradiation," *Journal of Nuclear Materials,* vol. 327, pp. 27-36, 2004.

[13] D. Porter, C. Lahm and R. Pahl, "Fuel constituent redistribution during the early stages of U-Pu-Zr irradiation," *Metallurgical Transactions A,* vol. 21A, p. 1871, 1990.

[14] C. Lahm, J. Keonig, R. Pahl, D. Porter and D. Crawford, "Experience with advanced driver fuels in EBR-II," *Journal of Nuclear Materials,* vol. 204, pp. 119-123, 1993.

[15] C. Lahm, J. Koenig, P. Betten, J. Bottcher, W. Lehto and B. Seidel, "EBR-II Driver Fuel Qualification for Loss-of-Flow and Loss-of-Heat-Sink Tests Without SCRAM," *Nuclear Engineering and Design,* vol. 101, pp. 25-34, 1987.

[16] D. Crawford, D. Porter and S. Hayes, "Fuels for sodium-cooled fast reactors: US perspective," *Journal of Nuclear Materials,* vol. 371, pp. 202-231, 2007.

[17] R. Baker, F. Bard, R. Leggett and A. Pitner, "Status of fuel, blanket, and absorber testing in the fast flux test facility," *Journal of Nuclear Materials,* vol. 204, pp. 109-118, 1993.

[18] L. Walters, B. Seidel and J. Kittel, "Performance of metallic fuels and blankets in liquid-metal fast breeder reactors," *Nuclear Technology,* vol. 65, pp. 179-231, 1984.

[19] A. Pitner and R. Baker, "Metal fuel test program in the FFTF," *Journal of Nuclear Materials,* vol. 204, pp. 124-130, 1993.

[20] A. Yacout, "Long-Life Metallic Fuel for the Super Safe, Small and Simple (4S) Reactor," Toshiba Corporation & Central Research Institute of Electric Power Industry, Argonne, 2008.

[21] R. Pahl, D. Porter, D. Crawford and L. Walters, "Irradiation behavior of metallic fast reactor fuels," *Journal of Nuclear Materials,* vol. 188, pp. 3-9, 1992.

[22] J. Sackett, "Operating and test experience with EBR-II, the IFR prototype," *Progress in Nuclear Energy,* vol. 31, pp. 111-129, 1997.

[23] H. Planchon, G. Golden and J. Sackett, "Demonstration of Passive Safety Features in EBR-II," 1987.

[24] H. Planchon, G. Golden, J. Sackett, D. Mohr, K. Chang, E. Feldman and P. Better, "Results and Implications of the Experimental Breeder Reactor II Inherent Safety Demonstration Tests," *Nuclear Engineering and Design ,* vol. 100, pp. 549-577, 1988.

[25] T. Bauer, A. Wright, W. Robinson, J. Holland and E. Rhodes, "Behavior of modern metallic fuel in TREAT transient overpower tests," *Nuclear Fuel Cycles,* vol. 92, p. 325, 1990.

[26] D. Burkes, R. Fielding, D. Porter, D. Crawford and M. Meyer, "A US perspective on fast reactor fabrication technology and experience part I: metal fuels and assembly design," *Journal of Nuclear Materials,* vol. 389, pp. 458-469, 2009.

[27] T. Ogata and T. Tsukada, "Engineering-scale development of injection casting technology for metal fuel cycle," in *Global 2007*, Boise, 2007.

[28] D. Burkes, R. Fielding and D. Porter, "Metallic fast reactor fuel fabrication for the global nuclear energy partnership," *Journal of Nuclear Materials,* vol. 392, pp. 158-163, 2009.

[29] T. Ogata, "Metal Fuel," in *Comprehensive Nuclear Materials*, Amsterdam, 2012.

[30] K. Marsden, "Report on the development of concepts for the advanced casting system in support of the development of a remotely operable research scale fuel fabrication facility for metal fuel," Idaho National Laboratory, Idaho Falls, 2007.

[31] C. Lee, S. Oh and H. Ryu, "Casting technology development for SFR metallic fuel," in *Proceedings of Global 2009*, Paris, 2009.

[32] K. Kim, S. Oh, J. Lee, Y. Woo, Y. Ko and C. Lee, "Concept of atomized metallic fuel for SFR," in *Transactions of the Korean Nuclear Society Autumn Meeting*, PeyongChang, 2007.

[33] T. Ogata and T. Mizuno, "Directions of metal fuel development for fast reactors," in *Proceedings of Global 2009*, Paris, 2009.

[34] C. Clark, G. Knighton, R. Fielding and N. Hallinan, "INL Laboratory Scale Atomizer," Idaho National Laboratory, Idaho Falls, 2010.

[35] J. Kim, J. Lee, K. Kim and C. Lee, "Preliminary study on the fabrication of particulate fuel through presureless sintering process," *Science and Technology of Nuclear Installations,* vol. 2016, 2016.

[36] K. Ho and S. Newman, "State of the art electrical discharge machining (EDM)," *International Journal of Machine Tools & Manufacture,* vol. 43, pp. 1287-1300.

[37] K. Gamble, R. Williamson, D. Schwen, Y. Zhang, S. Novascone and P. Medvedev, "BISON and MARMOT Development for Modeling Fast Reactor Fuel Performance," Idaho National Laboratory, 2015.

[38] A. Yacout and M. Billone, "Current Status of the LIFE Fast Reactors Fuel Perfomance Codes," in *International Conference on Fast Reactors and Related Fuel Cycles: Safe Technologies and Sustainable Scenarios*, Paris, 2013.

[39] T. Fanning, "The SAS4A/SASSYS-1 Safety Analysis Code System, ANL/NE-12/4," Argonne National Laboratory, 2012.

[40] D. Keiser, "The development of fuel cladding chemical interaction zones in irradiated U-Zr and U-Pu-Zr fuel elements with stainless steel cladding," in *Nuclear Reactors, Nuclear Fusion, and Fusion Engineering*, Hauppauge, NY: Nova Science, 2009.